Impact of the selenisation temperature on the structural and optical properties of CZTSe absorbers

J. Márquez-Prieto,[1,†] M.V. Yakushev,[2,3,4†] I. Forbes,[1] J. Krustok,[5] P.R. Edwards,[2]
V.D. Zhivulko,[6] O.M. Borodavchenko,[6] A.V. Mudryi,[6]
M. Dimitrievska,[7] V. Izquerdo-Roca,[7] N.M. Pearsall,[1] and R.W. Martin[2]

[1]*NPAG, Department of Physics and Electrical Engineering, Northumbria University, Newcastle upon Tyne NE1 8ST, UK*
[2]*Department of Physics, SUPA, University of Strathclyde, Glasgow G4 0NG, UK*
[3] *Ural Federal University, Ekaterinburg* 620002*, Russia*
[4]*Institute of Solid State Chemistry of the Russian Academy of Sciences, Ekaterinburg 620990, Russia*
[5] *Tallinn University of Technology, Ehitajate tee 5, Tallinn 19086, Estonia*
[6]*Scientific-Practical Material Research Centre of the National Academy of Sciences of Belarus, P.Brovki 19, Minsk 220072, Belarus*
[7] *Catalonia Institute for Energy Research, Jardins de les Dones de Negro 1, Sant Adria de Besos, Spain*

Corresponding author: michael.yakushev@strath.ac.uk tel. +44 141 548 3374
Keywords: $Cu_2ZnSnSe_4$, selenisation, optical spectroscopy, structure
Abstract

We present structural and optical spectroscopy studies of thin films of $Cu_2ZnSnSe_4$ (CZTSe) with strong copper deficiency deposited on Mo/Glass substrates and selenised at 450, 500 or 550^o C. Solar cells fabricated from these films demonstrated efficiencies up to 7.4% for selenisation at 500 ^{o}C. Structural analysis based on X-ray diffraction and Raman spectroscopy revealed the presence of $SnSe_2$ in the film selenised at 450 ^{o}C but not in the films selenised at higher temperatures. A progressive decrease of the Sn and Se content was observed as the selenisation temperature increased. Photoluminescence excitation was used to determine the bandgaps at 4.2 K. Detailed measurements of the temperature and excitation intensity dependencies of the photoluminescence spectra allow the recombination mechanisms of the observed emission bands to be identified as band-to-impurity and band-to-band transitions, and their evolution with selenisation temperature changes to be analysed. The strongest band-to-band transition is recorded in the PL spectra of the film selenised at 500 ^{o}C and can be observed from 6 K to room temperature. The compositional and structural changes in the films and their influence on the optoelectronic properties of CZTSe and solar cells are discussed.

1. Introduction

The semiconductor compound $Cu_2ZnSnSe_4$ (CZTSe) is a promising material for the absorber layer of sustainable thin-film solar cells, containing inexpensive and earth-crust-abundant elements, with the highest reported conversion efficiencies exceeding 11% [1]. Similarities of the lattice structure and electronic properties of CZTSe to those in $Cu(InGa)Se_2$ (CIGS) [2,3,4] provide an opportunity to facilitate the development of CZTSe-based solar cells by applying technological solutions originally developed for CIGS-based solar cells [2, 3].

The natural *p*-type doping of CZTSe is ascribed to intrinsic defects [2, 4], and therefore understanding of such defects can accelerate progress in the solar cell performance. Current knowledge of the electronic properties and especially of defect properties is mostly based on theoretical studies carried out using density functional theory [4, 5]. However there is significant value in providing experimental evidence to confirm the theoretical findings [6-12].

The reactive annealing used to form the absorber layer is one of the key steps in the fabrication of high performance solar cells. It is important to optimise the choice of chalcogen sources, type of precursor and a number of process parameters. A range of selenisation temperatures has been reported to be suitable for processing absorbers for highly efficient solar cells. The reactive annealing process in a 11.2% CZTSe solar cell, reported by IBM [1], was carried out at very high temperature (590 ^{o}C) whereas for a 10.4% CZTSe solar cell, reported by IMEC [13], the absorber layer was selenised at 460 ^{o}C. Therefore a comprehensive study of selenisation parameters and their relation to the electronic properties of the absorber layers and parameters of subsequent solar cells is needed to improve the CZTSe technology and understand the limitations of each process used.

Photoluminescence (PL) can be efficiently used to study defects in semiconductors [7,8,9,10,14]. Low temperature PL spectra of CZTSe thin films with strong Cu deficiency and Zn excess (compositional requirements for the absorber layer in high performance solar cells [4, 15, 16]) are dominated by a broad and asymmetrical band attributed to band tail related recombination [8, 9, 17]. Such spectra on their own however are not very informative. To gain a better understanding of the defect properties it is important to study correlations of spectroscopic parameters (resulting from detailed PL analysis spanning cryogenic and room temperatures) with the technological parameters of the fabrication processes used to produce the solar cells. Currently such correlations have only been reported for room temperature PL measurements [17] which offers limited information on defects and radiative recombination processes in the absorber layer.

To interpret data gained from PL measurements, it is essential to have reliable values of the bandgap E_g.

This can be obtained from photoluminescence excitation (PLE) data, which do not require a *p-n* junction and can be used to analyse films deposited on Mo coated glass [18].

In this paper we present a structural and optical spectroscopy study of thin films of CZTSe with strong copper deficiency deposited on Mo/glass substrates using three selenisation temperatures. These films were used to fabricate solar cells. We analyse the elemental composition, structural and optical spectroscopy properties of the CZTSe films and try to correlate these properties with the performance of the cells.

2. Experimental details

Precursor layers were simultaneously deposited on Mo-coated soda-lime glass substrates at room temperature by magnetron sputtering of high-purity copper (Cu), zinc (Zn) and tin (Sn). These precursors were selenised in graphite boxes by a two-step rapid thermal process for 5 and 15 minutes, respectively. Nitrogen at 850 mbar was used as background pressure. The first step was at 300 ^{o}C and the second at 450 ^{o}C, 500 ^{o}C and 550 ^{o}C for films 1, 2 and 3, respectively. More information on synthesis of compound films by selenisation of magnetron deposited precursors can be found elsewhere [19].

CdS buffer layers were grown using a standard chemical bath process after etching the films with a 10 wt % KCN solution for 30 seconds. Solar cells of 3×3 mm^2 in area were then fabricated by DC-magnetron deposition of ZnO/ZnO:Al transparent front contacts and mechanical scribing. The principal device parameters measured under simulated AM1.5 solar illumination (100 mW/cm^2, 25 ^{o}C) for cells fabricated from films 1 and 2 are shown in Table 1. The current density – voltage characteristics (J-V) measurements were performed by contacting the solar cells directly on the TCO front surface, since there was no metallic grid added. Electrical measurements could not be performed on film 3, where the Mo back contact was totally consumed in the selenisation step.

The morphology and elemental composition of the films were examined by scanning electron microscopy (SEM) and wavelength dispersive X-ray (WDX) microanalysis at 5 keV and 10 keV electron beam energies, respectively.

The structural properties and the presence of secondary phases were analysed by room temperature Raman scattering using a 532.0 nm excitation laser and LabRam HR800-UV spectrometer.

X-ray diffraction (XRD) measurements were carried out using a Siemens D-5000 diffractometer in the Bragg–Brentano geometry and a Cu K-$_{\alpha}$ radiation source (λ = 0.15406 nm).

A 1 m focal length single grating monochromator and the 514 nm line of a 300 mW Ar^+ laser were used for the photoluminescence (PL) measurements. A closed-cycle helium cryostat was employed to measure temperature dependence of the PL spectra at temperatures from 6 K to 300 K. The PL signal was detected by an InGaAs photomultiplier tube sensitive from 0.9 µm to 1.7 µm. A 400 W halogen tungsten lamp combined with a single grating monochromator (focal length of 0.3 m) was used as an excitation source for PLE measurements. A 0.6 m focal length single grating monochromator, an InGaAs photodiode sensitive from 0.9 µm to 1.9 µm and a liquid helium bath cryostat were used for the PLE measurements. More experimental details can be found in ref. [7,10].

3. Results:

a. Microstructure, elemental composition and device performance

The top SEM views of films 1, 2 and 3, are shown in Fig.1(a), (b) and (c), respectively. A gradual increase of the grain size can be seen as the selenisation temperature rises.

The elemental compositions of the films, determined by WDX as the average of 10-point linear scans are shown in Table 1. The ratios of copper to the Sn and Zn ([Cu]/[Zn+Sn]), Zn to Sn ([Zn]/[Sn]) and the ratio of Se to the sum of all the metals ([Se]/[Zn+Sn+Cu]) are also shown in Table 1 with standard deviations of the 10 measurements taken as the error bars. Each film has strong Cu deficiency and films 2 and 3 have a weak excess of Zn. Solar cells with similar composition of the CZTSe layers showing high open circuit voltage V_{OC} and efficiencies exceeding 8% have been previously reported [20]. The content of Cu can be seen increasing with rising selenisation temperature.

The XRD patterns of the absorber layers are shown in Fig. 2. The formation of tetragonal CZTSe is confirmed for the whole range of selenisation temperatures in agreement with previous studies [19, 21]. A prominent peak at 40^{o}, which is seen in the diffraction patterns can be attributed to metallic Mo used as a back contact. This peak is the most intense for film 1. As the selenisation temperature increases, the intensity of the peak decreases. It completely disappears for film 3 selenised at the highest temperature of 550 ^{o}C. The opposite trend occurs with the broad reflections at 32^{o} and 57^{o} attributed to $MoSe_2$ showing a gradual increase in the intensity as the selenisation temperature rises. The total conversion of the metallic Mo into $MoSe_2$ at 550 ^{o}C explains why a good electrical contact with the back of the device made from film 3 could not be achieved, making electrical characterization of this solar cell impossible. The diffractogram of film 1 also shows two narrow peaks at 14.4^{o} and 30.8^{o} which are consistent with the presence of $SnSe_2$ (PDF numbers: 01-089-2939 23-602).

Figure 3 shows normalised Raman spectra for the three films. All the peaks observed in the spectra with the exception of a peak at 184 cm^{-1} observed for Film 1, can be attributed to CZTSe phase [11]. Different possible phases have been considered for assignment of the peak at 184 cm^{-1}. Marcano *et al*. reported Raman spectra of the monoclinic Cu_2SnSe_3 (CTSe) [22], with the most intense peak appearing at 180 cm^{-1}. The most intense Raman peak for $SnSe_2$ has been experimentally

observed at 184 cm^{-1}. It was also theoretically predicted at 187 cm^{-1} [23]. The inset of Fig. 3 shows the evolution of the FWHM value of the A mode of CZTSe at 197 cm^{-1}. A progressive decrease in the FWHM values can be seen as the selenisation temperature increases. This reduction is associated with an improvement of the crystal quality, which reduces the possible presence of phonon confinement effect and increases the phonon lifetime (reduction of the dispersion in the phonon energies) [24].

Fig.4 shows the J-V characteristics of the solar cells fabricated from films 1 and 2, measured under AM1.5 illumination. Resulting efficiencies of 3.2% and 7.4%, respectively, and principal solar cell parameters are shown in Table 1. The cell, fabricated using film 2, has an V_{OC} of 421 meV, which is close to that in the current record CZTSe solar cell [1]. However the short circuit current density J_{SC} is lower than that in [1] by about 10 mA cm^{-2}. This difference can be partly due to the high thickness of the TCO layer (about 700 nm) in our cell. Such a thick layer was intentionally deposited to protect the device during the electrical measurements because no metallic grid was evaporated. The absence of an antireflective coating on our devices could increase the efficiency by about 1 % in absolute values.

b. PL and PLE analysis of the films

The 6 K PL spectra of the three films, measured at similar optical alignments and laser excitation, are shown in Fig.5 and reveal a high intensity, broad asymmetrical band P1 with the maximum at 0.934 eV (film 1), 0.944 eV (film 2) and 0.898 eV (film 3). The slope of the peak is greater on the high energy side compared to the low energy one. Features associated with water vapour absorption can be seen at 0.9 eV.

Although the XRD patterns, shown in Fig.5, and the Raman spectra, shown in Fig.3, suggest the presence of small quantities of the secondary phases $SnSe_2$ and $MoSe_2$ we attribute the P1 band in in the PL spectra of Fig.5 to CZTSe. Bulk forms of $SnSe_2$ reveal forbidden indirect transitions at 1.0 and 1.3 eV whereas an allowed direct transition appears at 2.0 eV [25]. Within the examined spectral region from 0.7 eV to 1.4 eV absorption as well as emission by $SnSe_2$ should be several orders of magnitude lower than that by CZTSe. Therefore we do not expect $SnSe_2$ to have any significant effect either in the PL or PLE spectra. Mono-layers of $MoSe_2$ show strong PL emission at 1.57 eV and a direct allowed bandgap of 1.58 eV [26]. However an increase of the number of layers reduces the PL intensity by several orders of magnitude, shifts the bandgap to 1.41 eV and makes it indirect [27]. $MoSe_2$ should not therefore have significant effects on the PL and PLE spectra. This is confirmed by our PL measurements of CZTSe thin films deposited simultaneously with those in the present study but on glass substrates [28]. The 6 K PL spectra from the films on glass reveal an asymmetric PL band at 0.94 eV very similar to those shown in Fig.5.

Increasing the selenisation temperature, from 450 ^{o}C to 500 ^{o}C, produces an increase in the band intensity, and a blue shift of about 10 meV in the spectral position, while leaving the full width at half maximum (FWHM) unchanged at 84 meV. Further temperature increase to 550 ^{o}C decreases the intensity beyond that at 450^{o}C, red shifts the spectral position by 46 meV with respect to that in film 2, and broadens the FWHM to 100 meV. Spectral positions and FWHM of the P1 bands in the films are shown in Table 3.

Fig.6 shows the excitation intensity dependence of the PL spectra for the three films. The integrated intensity *I(P)* of the P1 band increases with excitation laser power *P* as $I \sim P^k$ with a power coefficients of $k \approx 1.0$ for each film. Values of *k* smaller than unity are interpreted as a recombination involving localisation of the carriers at defects with levels inside the band gap whereas values greater than unity as a recombination not involving localisation at defect [24,30].

In all the three cases the P1 band shows significant shifts to higher energies with increasing laser power, whereas neither the FWHM nor the asymmetric shape of the P1 band changes. The rate of shift (*j* – shift) increases from 11 to 12 meV per decade of laser power as the selenisation temperature rises from 450 ^{o}C to 500 ^{o}C, suggesting a slight increase in the compensation level in film 2. A further rise in the selenisation temperature up to 550 ^{o}C increases the *j*-shift to 15 meV per decade, indicating a more significant increase in the compensation level.

Such significant *j*-shifts in P1, along with its asymmetric shape at low temperatures, are characteristics of band tail related recombination mechanisms [30, 31]. Tails in the electron and hole densities of states, at energies below the conduction band E_c, or above the valence band E_v, are formed in highly doped semiconductors by spatial potential fluctuations generated by high concentrations of randomly distributed charged defects [32].

The temperature dependence of the PL spectra is shown in Fig.7 on a logarithmic scale. It can be seen that the dominant P1 band gradually quenches by 135 K, 90 K and 160 K in film 1, 2 and 3, respectively. With rising temperature the P1 band reveals a clear red shift in all the films. Such shifts can be taken as a confirmation of the band tail related nature of this emission [30, 31]. Bands at 0.94 eV in low temperature PL spectra of CZTSe have been reported earlier [8, 10, 17, 33] and attributed to valence band tail related transitions.

A second band P2 can be seen emerging at 1 eV in the spectra at higher temperatures. This band can be seen at temperatures up to 230 K in film 1 and up to 300 K in films 2 and 3. Comparison of the spectral position of P2 with literature values of the bandgap (1.01 eV) measured in CZTSe film with Cu deficiency and Zn excess at room temperature, support a preliminary assignment as band to a band-to-band (BB) recombination of free electrons from the conduction band with free holes from the valence band [28]. The presence of the BB band in the PL spectra as an unresolved peak can also increase the *k* values.

PLE spectra, measured at 4.2 K to determine the bandgap of the films, are shown in Fig.8 and compared with PL spectra for the three films. The PLE spectra show broadening which suggests the presence of sub-bandgap absorption states associated with band tails. To take into account such a broadening the low energy sides of the PLE spectra, representing absorptance $\alpha(E)$, are fitted with sigmoidal shapes [34] $\alpha(E) = \alpha_0/(1 + exp(E_g - E)/\Delta E)$, where E_g is the bandgap and ΔE is a broadening parameter equivalent to the Urbach tailing energy [35]. The best fits for each film are shown in Fig.8 by red lines. Values of E_g, determined from fitting equation (1) to the PLE spectrum, are (1.05±0.01) eV, (1.03±0.01) eV and (1.05±0.01) eV, for films 1, 2 and 3, respectively. These bandgap energies suggest a high degree of ordering in the Cu-Zn plane of the CZTSe structure [36].

4. Analysis of the PL recombination mechanisms

The evolution of the normalised PL spectra in the three films with rising temperature is shown in Fig. 9 on a linear scale. The shape of the P1 band in all the three films can be seen to change from being significantly asymmetrical, with a sharp slope on the high energy side at low temperatures and a gentle slope on the low energy side, to Gaussian-like at temperatures above 100 K. Fig.9(a) and (c), corresponding to films 1 and 3 respectively, clearly show that the shape of the low energy side of P1 does not change. The high energy side becomes gentler making the band symmetrical. In Fig.8(b), corresponding to film 2, changes in the high energy side are obscured by the appearance of the P2 band at temperatures above 70 K.

The low-energy side of a band tail related band is defined by the density of states function of the valence band tail $\rho_v(\varepsilon)$ [30, 37] and depends neither on temperature nor on excitation intensity, as can be seen in Fig.6, 7 and 9.

The P2 band is evident in the linear scale PL spectra at different temperatures. In film 1, its intensity becomes significant at 135 K and in film 3 at 150 K, whereas in film 2 it can be resolved from 60 K and becomes dominant from 90 K. In the PL spectra shown in Fig.6 on a logarithmic scale, the P2 band can clearly be seen in the spectra of film 2 from 6 K whereas it is difficult to see this band in the 6 K spectra for films 1 and 3.

A low energy tail (LET) feature can be seen in the PL spectra in Fig.9(a), corresponding to film 1, at temperatures above 100 K. Its intensity becomes significant above 115 K. This LET quenches at temperatures above 230 K. The LET belongs to a deep low energy band with its maximum beyond the low energy limit of 0.9 μm in the InGaAs detector used. Neither film 2 nor film 3 reveals such a band in their PL spectra.

The temperature dependence of the spectral maxima for the P1 and P2 bands for the three films are shown in Fig.10(a). Although clear red shifts of the P1 band can be seen for all three films, their spectral magnitudes are quite different. The greatest shift of 84 meV is seen for P1 in film 1 as the temperature rises from 6 to 165 K; at higher temperatures P1 quenches. In the PL spectra of film 2 the P1 band redshifts by 19 meV reaching its spectral minimum at a much lower temperature of 75 K, then showing a blue shift at higher temperatures before quenching. In the PL spectra of film 3 the P1 band red shifts by 51 meV, reaching its maximum at 125 K, and then showing blue shifts at high temperatures.

In a highly doped semiconductor, the average distances between defects become smaller than their Bohr radii, causing the defect wave-functions to overlap [32]. The density of state (DOS) hole and electron masses, $m^*_h = 0.21m_0$ and $m^*_e = 0.08m_0$, respectively, (where m_0 is the free electron mass), determined from theoretical studies of CZTSe [5] suggest that holes are significantly heavier than electrons making the condition of high doping easier to satisfy for donors. The level of high doping by acceptors is usually much higher and the holes can be treated as classical particles. It is generally assumed that in the chalcopyrites [31, 38-40] and kesterites [8] the condition of high doping is satisfied for electrons and not satisfied for holes. At low temperatures, holes are captured in deep states of the valence band tail which acts like a hydrogenic acceptor.

Energy diagrams of the BT and BI transitions are shown in Fig.10(b). The figure also shows the density of states (DOS) for the conduction ρ_c and valence ρ_v bands as well as DOS of an acceptor level ρ_a participating in the BI transition for a semiconductor with spatial potential fluctuations. The P1 band may be a result of the band-to-tail (BT) recombination of free electrons from the quasi-Fermi level for electrons F_n with holes captured at levels within the valence band tail. At low temperatures, the holes are localised at deep tail states. Their probability of being released is low, whereas the probability of recombining with free electrons from the conduction band is quite high. Once the temperature rises, shallow valence band tail states release holes which participate in the BB transition whereas holes at deeper states stay localised. Their recombination with free electrons determines the red shift of the P1 band [30, 31]. The rate of the shift, the gradient of the temperature dependence of the P1 maximum in Fig.10 (a), and the temperature of the minimum all depends on the carrier concentration determined by the level of doping as well as excitation intensity.

A good approximation for the density of states of the holes localised at the valence band tail is given by the following expression:

$$\rho_v(\varepsilon) \sim exp(-(\varepsilon/\gamma)^2), \qquad (1)$$

where γ is the average depth of the valence band potential energy fluctuations. Therefore the low energy side of the BT band can be used to estimate γ [30, 31].

An alternative explanation of the P1 band could be the BI recombination of free electrons and holes captured at conventional acceptors with ionisation

energy I_a, if it is greater than the average tail depth γ as shown in Fig. 10(b). In materials with spatial potential fluctuations the BI band also has a characteristic asymmetric shape. It also red shifts at rising temperature as well as showing a significant blue shift at increasing excitation intensity [30, 38]. In such materials the band-to-impurity recombination includes two processes: BI_1, recombination of free holes captured at acceptor, and BI_2, recombination of holes first captured at the valence band tail. In the presence of band tails the hole density of states is distributed about the acceptor's activation energy, I_a, as:

$$\rho_a(\varepsilon) = (N_a / \sqrt{2\pi\gamma}) \exp[-(\varepsilon - I_a)/2\gamma^2], \qquad (2)$$

where N_a is the acceptor concentration [30, 38]. Similarly to the BT band, the density of states determines the shape of the low energy side of the BI band, which can be used to estimate γ. To identify the recombination mechanism of the P1 band, average tail depths γ of 24, 24 and 27 meV have been estimated from the low energy slopes of the P1 band PL spectra at 6 K [30, 31]. These values are collected in Table 3.

To analyse temperature quenching of the P1 band, the PL spectra at different temperatures were fitted with three Gaussian profiles to match the high energy side of P1, P2 and HT. Examples of such fits are shown in Fig.11 for spectra, taken at 6 K. It can be seen that the high energy sides are well fitted by the lines. Therefore we can use such fits to improve the accuracy of calculations of the P1 band integral intensity at temperatures, where the intensity of P2 and HT are significant with respect to that of P1, by subtracting the Gaussians representing these bands from the PL spectra. However we can determine their reliable spectral positions or trace their temperature dependencies only if the P1 band is quenched and P2 is resolved as shown in Fig.7, 9 and 10(a). It can be seen in Fig.11 that the relative intensity of the P2 Gaussian for film 2 is significantly higher than for the other films.

Arrhenius analysis of the P1 band temperature quenching was carried out by calculating integrated intensities after the subtraction of the Gaussians representing the P2 and LET features. The resulting intensities for the three films are plotted in Fig.12 on an Arrhenius scale. The best fits, shown by the lines, are achieved for one recombination channel assuming the temperature dependent hole capture cross section proposed in [41]:

$$I(T) = I_0/(1 + A_1 T^{3/2} + A_2 T^{3/2} \exp(-E_a/k_B T)), \qquad (3)$$

where I_0 is the P1 band integrated intensity at the lowest temperature of 6 K, and A_1 and A_2 are process rate parameters. Activation energies E_a of (42 ± 6) meV, (63 ± 8) meV and (41 ± 2) meV are determined for the P1 band in the PL spectra of films 1, 2 and 3, respectively.

A BT transition can be described by the effective ionisation energy E_a of acceptor-like states in the valence band tail determining the BT band emission. In this case E_a should be a fraction of the average tail depth γ. However the determined values of E_a are greater than γ suggesting that the P1 band is more likely to be associated with BI transitions, the recombination of free electrons with holes localised by conventional acceptors with bandgap energy level position spread by spatial potential fluctuations.

The P2 band temperature dependencies, shown in Fig.7, 9 and 11(a) for the three films, are very different. In the PL spectra of film 1 the P2 band, with the maximum at 0.99 eV, emerges from the P1 band and then quenches at temperatures just above 200 K showing little shift in its spectral position. Although it is not resolved in the low temperature spectra in Fig.7 and 9, the fitting of the high energy side of the spectrum at 6 K, shown in Fig.11(a), requires its presence at an estimated energy of 1.027 eV to fill the difference between the spectrum and the fit. This spectral energy is in good agreement with the PLE determined E_g value of 1.04 eV measured at 4.2 K.

In film 2 the P2 transition can be seen on the logarithmic scale spectra from 6 K in Fig.7(b). In Fig.11(b) the fitting of the spectrum to three Gaussians (P1, P2, HT) is compared with a similar fitting with the two Gaussian (P1 and HT) fit, demonstrating the necessity of a P2 peak. Although unresolved, the P2 spectral energy in film 2 at 1.045 meV is greater than that in film 1 and in good agreement with the E_g determined from the PLE experiments. Assuming that the P2 band is the BB recombination we can use this assignment to trace the temperature dependence to follow that of the bandgap. The red shift of 33 meV over a temperatures change of 95 - 300 K is close to that of 40 meV observed for excitonic quality CZTSe over a slightly greater temperature change from 4 to 300 K [10] but exceeds the 20 meV determined by spectroscopic ellipsometry in CZTSe films with smaller Cu deficiency and Zn excess [42].

Although a resolved P2 band at 0.964 eV emerges in film 3 at 160 K, its unresolved presence can be seen at 1.027 eV in the 6 K PL spectrum shown in Fig.10(c) with and without the Gaussian representing the P2 band. The BB band shows a blue shift from 0.964 to 1.012 eV with temperature increasing from 160 K to 300 K. According to [30], the temperature dependence of the BB band in semiconductors with a high level of doping can be described at high temperatures by:

$$E_{BB}(T) \sim E_g(T) - k_B T \ln(2(F_n - E_c)/k_B T), \qquad (4)$$

where F_c and F_n the quasi-Fermi levels for electrons and holes, respectively. Therefore at small values of $F_n - E_c$, the electron kinetic energy, E_{BB}, can shift to higher energies with rising temperature as has been demonstrated for $Cu(InGa)Se_2$ single crystals [31].

The spectral energy of the P2 band in the PL spectra of film 3 is noticeably smaller than the value of E_g = 1.05 eV determined by PLE. In comparing the spectral energy of P2 gained from PL measurements with E_g from measuring absorption, we should take in account that PL emission has a polaron nature due to interaction of the excited electrons and holes with

optical mode phonons in crystal lattices. Such an interaction slightly increases the electron and hole masses resulting in a red shift of the PL bands in comparison with absorption measurements [16, 30, 31, 43]. The spectral position of BB in semiconductors highly doped with donors depends on the quasi-Fermi level for electrons F_n [39].

5. Discussion

The significant increase in the performance for the films selenised at 500 ^{o}C compared to 450^{o}C may be due to the fact that, within the detection limits of the techniques used in this study, no secondary phases could be detected for that sample. In addition, an apparent grain growth with temperature, observed in the SEM top view images and the Raman results previously presented, indicated an increase of the crystalline quality. All the three films show significant copper deficiency with [Cu]/[Zn+Sn] of about 0.8. Combining such a deficiency with significant zinc excess in films 2 and 3, where Zn/Sn is about 1.2, the off-stoichiometric CZTSe will be of the group A-type, where electrically neutral defect clusters V_{Cu}+Zn_{Cu} are expected to be present in high concentration [20, 44]. Selenisation or annealing of CZTSe results in a loss of tin [16, 45]. A reduction of the Sn content with increasing selenisation temperature can be seen in the [Zn]/[Sn] ratios in Table 1. At annealing temperatures of 500 ^{o}C and 550 ^{o}C, decreasing tin content, gradually changes the [Zn]/[Sn] ratio towards zinc excess, increasing the [Cu]/[Zn+Sn] ratio. This is also consistent with the changes in Fig. 2 and Fig 3, where the XRD patterns and Raman spectra show evidence of the presence of $SnSe_2$ in film 1 whereas in films 2 and 3 at higher selenisation temperatures this phase is not detected.

A significant reduction in the concentration of $SnSe_2$ in film 2 (beyond the sensitivity of our XRD and Raman analysis) might be at least partly responsible for the observed 14% rise in J_{sc} and 25% rise in V_{oc} after the selenisation temperature changed from 450 ^{o}C to 500 ^{o}C due to the shunting effect of this phase [46].

The increase in the performance might also be correlated with the appearance of $MoSe_2$ peaks in the XRD patterns for the films selenised at 500 ^{o}C and 550 ^{o}C. Comparing the average depth of potential fluctuations γ in the films deposited on glass (γ = 37 meV [28]) and on molybdenum (γ = 24 meV in the present study) suggests improvements in the material quality when CZTSe is deposited on Mo. Higher selenisation temperatures, however, tends to reverse these improvements, so after the 550 ^{o}C selenisation γ increases to 27 meV.

The gradual decrease of the Se content with increasing selenisation temperature presented in Table 1 can be associated with the decomposition of the kesterite phase [45]. An increase of the concentration of selenium vacancies V_{Se} can be induced by this decomposition, which according to Chen *et al.* [4] is a deep donor. In the case of Cu_2ZnSnS_4, it has been theoretically predicted that at high temperatures, the formation energy of sulphur vacancies V_S is low and the concentration of this defect can be increased up to $2x10^{19}$ cm^{-3} [47,48].

Peaks of $SnSe_2$ can be identified in the XRD pattern for film 1. The Raman data also confirm the presence of $SnSe_2$ in this film. The increase in the selenisation temperature from 450 to 500^{o}C results in the disappearance of the $SnSe_2$ in film 2 and film 3. The temperature rise from 500 to 550^{o}C increases the relative intensity of the 172 cm^{-1} peak in the Raman spectrum in Fig.3. Such an increase can be interpreted as a reduction of the concentration of the defect complexes V_{Cu}+Zn_{Cu} [11, 19, 20], being consistent with the increase of the Cu content shown in Table 1.

The structural quality of semiconductors can be compared by the integrated PL intensity (IPLI) measured at similar conditions [14]. The higher the intensity, the lower is the level of non-radiative recombination and scattering of photo-excited electrons and holes by defects. Such a criterion is also valid for semiconductors used in the solar cell absorber layer [16, 49]. This pattern can be seen in Fig.4 where film 2, used for 7.4% efficiency solar cells, shows a significantly higher PL intensity at 6 K (by a factor of 1.8 in terms of IPLI ratios) than film 1. Film 3 shows significantly lower PL intensity than film 2 (by a factor of 2.3 in terms of IPLI ratios). This trend suggests that a solar cell made from film 3, if the problem of Mo contact is solved, would be less efficient than those made from film 1 and 2.

Non-radiative recombination can occur via deep defects in the bandgap limiting the PL yield [50]. An increase of the concentration of V_{Se}, due to the observed decrease of the Se content in this sample as the temperature rises from 500 ^{o}C to 550 ^{o}C, can explain the decrease of the PL intensity that we observe for the sample synthesised at 550 ^{o}C.

Defect concentrations in semiconductors can be estimated by examining the type of radiative recombination in low temperature PL spectra. For the highest quality materials (defect concentrations below 10^{15} cm^{-3}), such spectra show only sharp peaks of excitonic features and resolved DAP lines [51]. At doping levels above 10^{17} cm^{-3}, no excitons can be found in the PL spectra whereas sharp DAP lines merge into broader free-to-bound and DAP transitions. At higher donor doping level, the low temperature PL spectra are dominated by a broad band with a characteristic asymmetrical shape whose low energy side is defined by the density of states in the valence band tail. Increasing the average depth of potential fluctuations makes the band broader. The average depth of potential fluctuations in film 3 is significantly greater than that in films 1 and 2, which is consistent with the observed increase in the FWHM from 80 to 100 meV as shown in Table.2.

The determined activation energies are related to ionisation energies of the defects responsible for the BI band. We can speculate that in film 1, selenised at 450 ^{o}C, an activation energy of 43 meV might be associated with the acceptor V_{Cu}, which is supported by

theoretical studies [4] and consistent with the elemental composition showing significant copper deficiency along with a small deficit of zinc. In film 2 the activation energy significantly increases up to 63 meV which suggests a possible change in the acceptor. We speculate that this activation energy might be associated to the antisite defect Zn_{Sn} which has also been proposed by theory [4] and likely to be present under zinc excess conditions. Such a change in the acceptor seems to be beneficial. However the demonstrated improvement in the solar cell performance could be an effect of the general improvement of the structural quality indicated by higher PL intensity in general and higher intensity of the P2 band. The further increase in the selenisation temperature to 550^{o} C resulted in a significant decrease of E_a to 41 meV, which might be associated with another change in the nature of the main acceptor.

The determined by PLE measurements bandgaps over 1.00 eV in all the films might be associated with the presence of high populations of the defect complex V_{Cu}+Zn_{Cu} which restrain the Cu/Zn disorder [12].

The presence of the BB transition (the P2 band) in the low temperature PL spectra of all the three films indicates that the level of non-radiative recombination is relatively low. The highest intensity of P2 relative to P1 is in film 2, as shown in Fig.11, and its spectral energy at 1.045 eV, the greatest amongst the three films, suggest that its spectral position and relative intensity correlate with the improved solar cell performance.

6. Conclusion

We present a structural and optical spectroscopy study of CZTSe absorber layers with strong copper deficiency fabricated by the selenisation at 450, 500 and 550 ^{o}C of Cu-Zn-Sn precursor layers on Mo/glass substrates. The solar cells fabricated from these absorbers showed conversion efficiencies of 3.2% for the selenisation at 450 ^{o}C and 7.4% for the selenisation at 500 ^{o}C. The elemental composition of these absorbers reveals a monotonic decrease of the Sn and Se content with increasing the selenisation temperature. The detailed temperature and excitation intensity dependence analysis of the PL spectra as well as PLE determined measurements of the bandgap allowed us to identify the recombination mechanisms of the main emission bands as band-to-impurity (BI) and band-to-band (BB). In the three films, the BB band can be seen from 6 K. In the PL spectra of the film resulting in the 7.4% efficient solar cell, the BB emission is the most intense and can be seen from 6 K up to room temperature.

Acknowledgement

This work was supported by the EPSRC, Royal Society, BRFFR (F15IC-025), the US Civilian Research & Development Foundation (CRDF Global № RUE2-7105EK13) and the Ural Branch of RAS (13CRDF16), RFBR (14-02-00080, 14-03-00121, UB RAS 15-20-3-11), Marie Curie Training Network (ITN), "KESTCELLS", FP7/2007-2013 grant 316488, IUT 19-28 of the Estonian Ministry of Education and Research, FP7 CHEETAH grant 609788, the European Union through the European Regional Development Fund, Project TK141 and by Act 211 of Government of Russia 02.A03.21.0006.

Author information

Corresponding Author

*E-mail: michael.yakushev@strath.ac.uk

Author Contributions

†These authors contributed equally.

References

[1] Y.S. Lee, T. Gershon, O. Gunawan, T.K. Todorov, T. Gokmen, Y. Virgus, S. Guha, $Cu_2ZnSnSe_4$ Thin-Film Solar Cells by Thermal Co-evaporation with 11.6% Efficiency and Improved Minority Carrier Diffusion Length, Advanced Energy Materials, 12 (2015) 1401372-4.

[2] S. Siebentritt, S. Schorr, Kesterites - a challenging material for solar cells, Prog Photovoltaics, 20 (2012) 512-519.

[3] M.J. Romero, H. Du, G. Teeter, Y. Yan, M.M. Al-Jassim, Comparative study of the luminescence and intrinsic point defects in the kesterite Cu_2ZnSnS_4 and chalcopyrite $Cu(In,Ga)Se_2$ thin films used in photovoltaic applications, Physical Review B, 84 (2011) 165324-5.

[4] S. Chen, A. Walsh, X.G. Gong, S.H. Wei, Classification of lattice defects in the kesterite Cu_2ZnSnS_4 and $Cu_2ZnSnSe_4$ earth-abundant solar cell absorbers, Advanced materials, 25 (2013) 1522-1539.

[5] C. Persson, Electronic and optical properties of Cu_2ZnSnS_4 and $Cu_2ZnSnSe_4$, Journal of Applied Physics, 107 (2010) 053710-8.

[6] S. Schorr, The crystal structure of kesterite type compounds: A neutron and X-ray diffraction study, Solar Energy Materials and Solar Cells, 95 (2011) 1482-1488.

[7] F. Luckert, D.I. Hamilton, M.V. Yakushev, N.S. Beattie, G. Zoppi, M. Moynihan, I. Forbes, A.V. Karotki, A.V. Mudryi, M. Grossberg, J. Krustok, R.W. Martin, Optical properties of high quality $Cu_2ZnSnSe_4$ thin films, Applied Physics Letters, 99 (2011) 062104-3.

[8] M. Grossberg, J. Krustok, K. Timmo, M. Altosaar, Radiative recombination in $Cu_2ZnSnSe_4$ monograins studied by photoluminescence spectroscopy, Thin Solid Films, 517 (2009) 2489-2492.

[9] S. Oueslati, G. Brammertz, M. Buffiere, C. Koble, T. Oualid, M. Meuris, J. Poortmans, Photoluminescence study and observation of unusual optical transitions in $Cu_2ZnSnSe_4$/CdS/ZnO solar cells, Solar Energy Materials and Solar Cells, 134 (2015) 340-345.

[10] M.V. Yakushev, I. Forbes, A.V. Mudryi, M. Grossberg, J. Krustok, N.S. Beattie, M. Moynihan, A. Rockett, R.W. Martin, Optical spectroscopy studies of

$Cu_2ZnSnSe_4$ thin films, Thin Solid Films, 582 (2015) 154-157.
[11] M. Dimitrievska, A. Fairbrother, E. Saucedo, A. Perez-Rodriguez, V. Izquierdo-Roca, Influence of compositionally induced defects on the vibrational properties of device grade $Cu_2ZnSnSe_4$ absorbers for kesterite based solar cells, Applied Physics Letters, 106 (2015) 073903-4.
[12] M. Paris, L. Choubrac, A. Lafond, C. Guillot-Deudon, S. Jobic, Solid-state NMR and Raman spectroscopy to address the local structure of defects and the tricky issue of the Cu/Zn disorder in Cu-poor, Zn-rich CZTS materials, Inorganic chemistry, 53 (2014) 8646-8653.
[13] S. Oueslati, G. Brammertz, M. Buffière, H. ElAnzeery, O. Touayar, C. Köble, J. Bekaert, M. Meuris, J. Poortmans, Physical and electrical characterization of high-performance $Cu_2ZnSnSe_4$ based thin film solar cells, Thin Solid Films, 582 (2015) 224-228.
[14] H.B. Bebb, E. Williams, Semiconductors and Semimetals, Academic Press, New York, 8 (1972) 181.
[15] M. Dimitrievska, A. Fairbrother, V. Izquierdo-Roca, A. Pérez-Rodríguez, E. Saucedo, Two ideal compositions for kesterite-based solar cell devices, in: Photovoltaic Specialist Conference (PVSC), 2014 IEEE 40th, IEEE, 2014, 2307-2309.
[16] A.D. Collord, H. Xin, H.W. Hillhouse, Combinatorial Exploration of the Effects of Intrinsic and Extrinsic Defects in Cu2ZnSn(S,Se)4, IEEE Journal of Photovoltaics, 5 (2015) 288-298.
[17] A. Redinger, K. Hones, X. Fontane, V. Izquierdo-Roca, E. Saucedo, N. Valle, A. Perez-Rodriguez, S. Siebentritt, Detection of a ZnSe secondary phase in coevaporated $Cu_2ZnSnSe_4$ thin films, Applied Physics Letters, 98 (2011) 101907-3.
[18] L. Q. Phuong, M. Okano, G. Yamashita, M. Nagai, M. Ashida, A. Nagaoka,K. Yoshino, and Y. Kanemitsu Free-carrier dynamics and band tails in $Cu_2ZnSn(S_xSe_{1-x})_4$: Evaluation of factors determining solar cell efficiency Phys. Rev. B 92, (2015) 115204-7.
[19] J. Marquez-Prieto, Y. Ren, R.W. Miles, N. Pearsall, I. Forbes, The influence of precursor Cu content and two-stage processing conditions on the microstructure of $Cu_2ZnSnSe_4$, Thin Solid Films, 582 (2015) 220-223.
[20] J. Márquez, M. Neuschitzer, M. Dimitrievska, R. Gunder, S. Haass, M. Werner, Y.E. Romanyuk, S. Schorr, N.M. Pearsall, I. Forbes, Systematic compositional changes and their influence on lattice and optoelectronic properties of $Cu_2ZnSnSe_4$ kesterite solar cells, Solar Energy Materials and Solar Cells, 144 (2016) 579-585.
[21] J. Marquez-Prieto, I. Forbes, Evolution of phases in two-stage vacuum processed thin film $Cu_2ZnSnSe_4$ absorber layers, Materials Research Innovations, 18 (2014) 515-518.
[22] G. Marcano, C. Rincon, S.A. Lopez, G.S. Perez, J.L. Herrera-Perez, J.G. Mendoza-Alvarez, P. Rodriguez, Raman spectrum of monoclinic semiconductor Cu_2SnSe_3, Solid State Communications, 151 (2011) 84-86.
[23] A.J. Smith, P.E. Meek, W.Y. Liang, Raman scattering studies of SnS_2 and $SnSe_2$, Journal of Physics C: Solid State Physics, 10 (1977) 1321-1333.
[24] M. Dimitrievska, A. Fairbrother, A. Perez-Rodriguez, E. Saucedo, V. Izquierdo-Roca, Raman scattering crystalline assessment of polycrystalline Cu_2ZnSnS_4 thin films for sustainable photovoltaic technologies: Phonon confinement model, Acta Materialia, 70 (2014) 272-280.
[25] B.L. Evans, R.A. Hazelwood, Optical and electric properties of $SnSe_2$, Brit. J. Appl. Phys /J. Phys. D/ 2 (1969) 1507-1516.
[26] P. Tonndorf, R. Schmidt, P. Böttger, X. Zhang, J. Börner, A. Liebig, M. Albrecht, C. Kloc, O. Gordan, D. R. T. Zahn, S. M. de Vasconcellos, and R. Bratschitsch, Photoluminescence emission and Raman response of monolayer MoS_2, $MoSe_2$, and WSe_2, Optical Express, 21 (2013) 4908-4916
[27] Y. Zhang, TR. Chang, B. Zhou, YT. Cui, H. Yan, ZK. Liu, F. Schmitt, J. Lee, R. Moore, YL. Chen, H. Lin, HT. Jeng, SK. Mo, Z. Hussain, A. Bansil, ZX. Shen, Direct observation of the transition from indirect to direct bandgap in atomically thin epitaxial $MoSe_2$, Nature Technology, 9 (2014) 111-115.
[28] M.V. Yakushev, J. Márquez-Prieto, I. Forbes, P.R. Edwards, V.D. Zhivulko, A.V. Mudryi, J. Krustok, R.W. Martin, Radiative recombination in $Cu_2ZnSnSe_4$ thin films with Cu deficiency and Zn excess, Journal of Physics D: Applied Physics, 48, 2015, 475109-7.
[29] T. Schmidt, K. Lischka, W. Zulehner, Excitation-power dependence of the near-band-edge photoluminescence of semiconductors Phys. Rev. B 45, (1992) 8989-8994.
[30] A.P. Levanyuk, V.V. Osipov, Edge Luminescence of the Direct Gap Semiconductors, Usp. Fiz. Nauk., 133 (1981) 427-477.
[31] J. Krustok, H. Collan, M. Yakushev, K. Hjelt, The role of spatial potential fluctuations in the shape of the PL bands of multinary semiconductor compounds, Physica Scripta, T79 (1999) 179-182.
[32] B. Shklovskii, A. Efros, Electronic Properties of Doped Semiconductors. 1984, in, Springer, Berlin.
[33] F. Luckert, M. Yakushev, R. Martin, N. Beattie, G. Zoppi, M. Moynihan, I. Forbes, A. Mudryi, A. Karotki, J. Krustok, Optical Properties of Thin Films of $Cu_2ZnSnSe_4$ Fabricated by Sequential Deposition and Selenisation, The Solar Energy Society UK, (2010) 29-32.
[34] K.P. O'Donnell, R.W. Martin, P. G. Middleton, Origin of Luminescence from InGaN Diodes, Phys. Rev. Lett. 82, (1999) 237-240.
[35] F. Urbach, The long-wavelength edge of photographic sensitivity and of the electronic absorption of solids, Physical Review, 92 (1953) 1324.
[36] G. Rey, A. Redinger, J.S. Ler, T.P. Weiss, M. Thevenin, M. Guennou, B. El Adib, S. Siebentritt, The band gap of $Cu_2ZnSnSe_4$: Effect of order-disorder, Applied Physics Letters, 105 (2014) 112106-4.
[37] R. Bhattacharya, B. Pal, B. Bansal, On conversion of luminescence into absorption and the van

Roosbroeck-Shockley relation, Applied Physics Letters, 100 (2012) 222103-4.
[38] A. Jagomagi, J. Krustok, J. Raudoja, M. Grossberg, M. Danilson, M. Yakushev, Photoluminescence studies of heavily doped $CuInTe_2$ crystals, Physica B, 337 (2003) 369-374.
[39] I. Dirnstorfer, M. Wagner, D.M. Hofmann, M.D. Lampert, F. Karg, B.K. Meyer, Characterization of $CuIn(Ga)Se_2$ Thin Films, physica status solidi (a), 168 (1998) 163-175.
[40] M.V. Yakushev, A.V. Mudryi, V.F. Gremenok, E.P. Zaretskaya, V.B. Zalesski, Y. Feofanov, R.W. Martin, Influence of growth conditions on the structural quality of $Cu(InGa)Se_2$ and $CuInSe_2$ thin films, Thin Solid Films, 451-452 (2004) 133-136.
[41] J. Krustok, H. Collan, K. Hjelt, Does the low-temperature Arrhenius plot of the photoluminescence intensity in CdTe point towards an erroneous activation energy?, Journal of Applied Physics, 81 (1997) 1442-1445.
[42] S.G. Choi, T.J. Kim, S.Y. Hwang, J. Li, C. Persson, Y.D. Kim, S.H. Wei, I.L. Repins, Temperature dependent band-gap energy for $Cu_2ZnSnSe_4$: A spectroscopic ellipsometric study, Solar Energy Materials and Solar Cells, 130 (2014) 375-379.
[43] H. Fröhlich, Electrons in lattice fields, Advances in Physics, 3 (1954) 325-361.
[44] A. Lafond, L. Choubrac, C. Guillot-Deudon, P. Deniard, S. Jobic, Crystal Structures of Photovoltaic Chalcogenides, an Intricate Puzzle to Solve: the Cases of CIGSe and CZTS Materials, Zeitschrift Fur Anorganische Und Allgemeine Chemie, 638 (2012) 2571-2577.
[45] J.J. Scragg, P.J. Dale, D. Colombara, L.M. Peter, Thermodynamic aspects of the synthesis of thin-film materials for solar cells, Chemphyschem : a European journal of chemical physics and physical chemistry, 13 (2012) 3035-3046.
[46] S. Temgoua, R. Bodeux, N. Naghavi, S. Delbos, Effects of $SnSe_2$ secondary phases on the efficiency of $Cu2ZnSn(S_x,Se_{1-x})_4$ based solar cells, Thin Solid Films, 582 (2015) 215-219.)
[47] J.J. Scragg, T. Ericson, T. Kubart, M. Edoff, C. Platzer-Bjorkman, Chemical Insights into the Instability of Cu_2ZnSnS_4 Films during Annealing, Chemistry of Materials, 23 (2011) 4625-4633.
[48] V. Kosyak, N.B.M. Amiri, A.V. Postnikov, M.A. Scarpulla, Model of native point defect equilibrium in Cu_2ZnSnS_4 and application to one-zone annealing, Journal of Applied Physics, 114 (2013) 124501-16.
[49] W. Shockley, H.J. Queisser, Detailed Balance Limit of Efficiency of p-n Junction Solar Cells, Journal of Applied Physics, 32 (1961) 510-519.
[50] T. Unold, L. Gütay, Photoluminescence Analysis of Thin-Film Solar Cells, in: Advanced Characterization Techniques for Thin Film Solar Cells, Wiley-VCH Verlag GmbH & Co. KGaA, 2011, pp. 151-175.
[51] E.H. Bogardus, H.B. Bebb, Bound-Exciton, Free-Exciton, Band-Acceptor, Donor-Acceptor, and Auger Recombination in GaAs, Physical Review, 176 (1968) 993-1002.

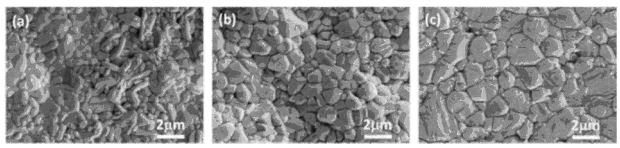

Fig.1. Top view SEM micrographs of the as deposited films 1 (a), 2 (b) and 3 (c) selenised at 450, 500 and 550°C, respectively.

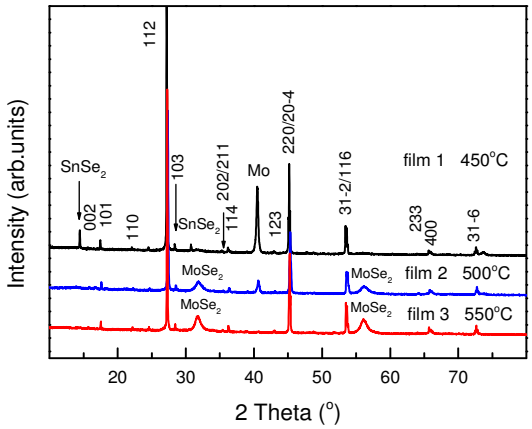

Fig.2. XRD patterns of CZTSe films on Mo coated glass selenised at different temperatures.

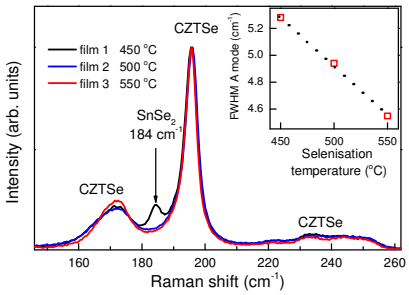

Fig.3. Raman spectra of the CZTSe thin films. The inset shows the variation of the FWHM of the most intense CZTSe mode.

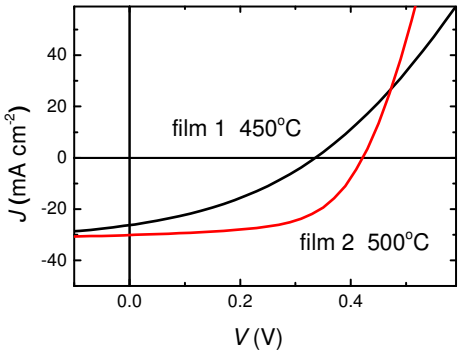

Fig.4. Current density – voltage (JV) curves of the best solar cells made of film 1 (450 °C) and 2 (500°C) (a).

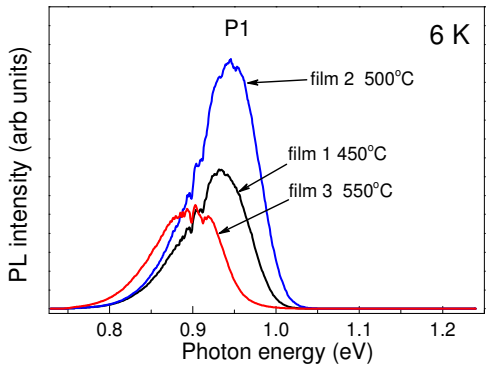

Fig.5. PL spectra from the films measured at 6 K, 0.053 W/cm^2 excitation and similar optical alignment.

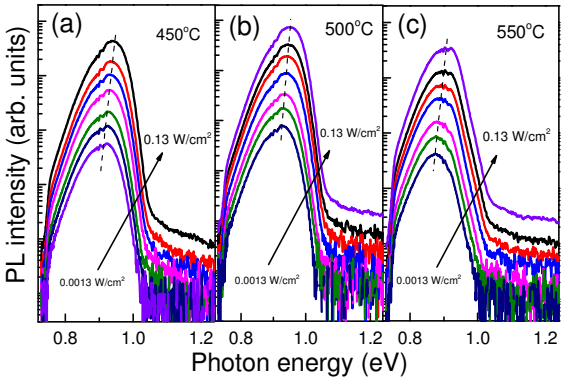

Fig.6. Excitation intensity dependencies of PL spectra in film 1 (a), film 2 (b) and film 3 (c) measured at 6 K.

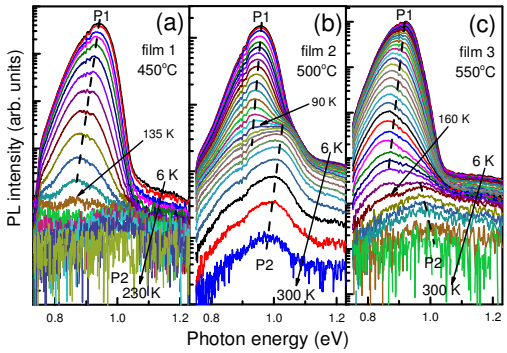

Fig.7. Temperature dependencies of the PL spectra in film 1 (a), film 2 (b) and film 3 (c).

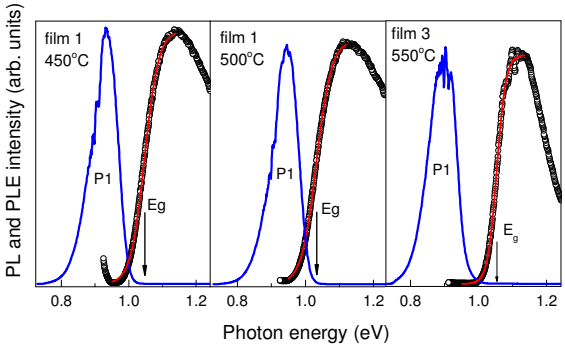

Fig.8. PLE spectra (measured at the maximum of the P1 band) and PL spectra of film 1 (a), film 2 (b) and film 3 (c) measured at 4.2 K. Red lines are the results of fitting.

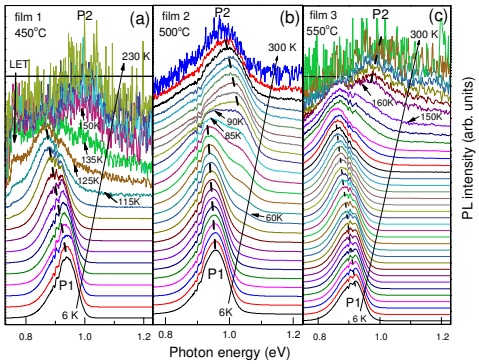

Fig.9. Evolution of the normalised PL spectra. The spectra are shifted along the y-axis for clarity.

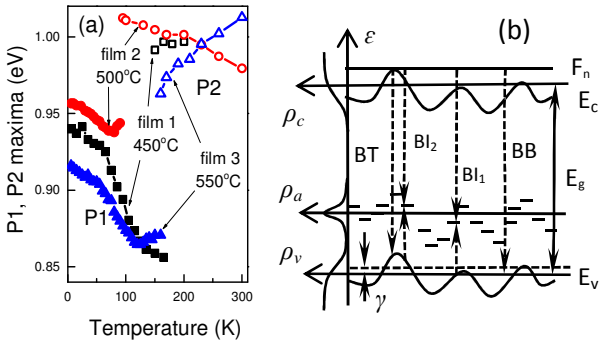

Fig.10. Temperature dependence of the spectral maxima of the P1 and P2 bands (a), density of states (DOS) for the conduction ρ_c and valence ρ_v bands as well as DOS of an acceptor level ρ_a in a semiconductor with potential fluctuations and energy diagram of band-to-tail (BT) and band-to-impurity (BI) recombination mechanisms shown by the dashed arrows (b).

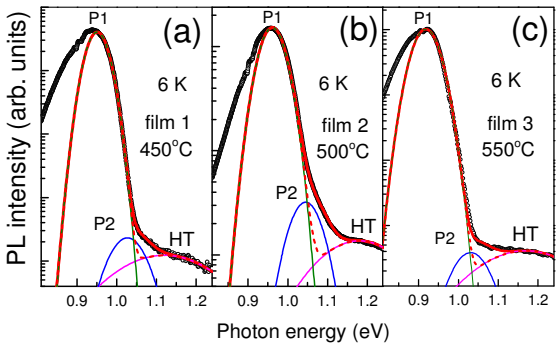

Fig.11. Fitting of the PL spectrum at 6 K with Gaussians representing P1, P2 and HT bands for film 1 (a), films 2 (b), films 3 (c). The solid red curves are the sums of the three Gaussians, the red dashed curves are fit with only two Gaussians representing P1 and HT but without P2.

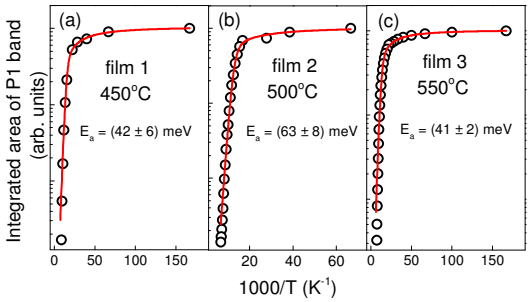

Fig.12. Arrhenius plots of the P1 band integrated intensities for film 1 (a), film (2), film (3).

Table 1. WDX elemental composition of the films.

Film	1	2	3
Temp. (°C)	450	500	550
Cu (at %)	21.1	21.8	22.6
Zn (at %)	13.2	15.2	14.8
Sn (at %)	14.6	12.9	12.6
Se (at %)	51.1	50.1	49.8
[Cu]/[Zn+Sn]	0.76± 0.08	0.78± 0.10	0.83± 0.04
[Zn]/[Sn]	0.92± 0.17	1.18± 0.02	1.17± 0.06
[Se]/[Cu+Zn+Sn]	1.16± 0.02	1.00± 0.01	0.99± 0.01

Table 2. J-V characteristic of the solar cells prepared with films 1 and 2.

Film	1	2
Temp. (°C)	450	500
Voc (mV)	336	421
Jsc (mA/cm2)	26.5	30.2
FF	35.2	58.0
η (%)	3.2	7.4

Table 3. Spectral characteristics of the P1 PL band measured at 6 K, bandgaps E_g measured by PLE, average depths of potential fluctuations γ and activation energies E_a of the P1 band temperature quenching for the films 1, 2 and 3.

Film	1	2	3
Selenisation temp. (°C)	450	500	550
P1 E_{max} (eV)	0.934	0.944	0.898
P1 FWHM (meV)	84	84	100
P1 j-shift (meV/decade)	11	12	15
E_g (eV) (PLE)	1.05	1.03	1.05
γ (meV)	24	24	27
E_a(meV)	42	63	41